Synthesis and Characterisation of Luminescent $[Cr^{III}_2L(\mu\text{-carboxylato})]^{3+}$ Complexes with High-Spin $S = 3$ Ground States ($L = N_6S_2$ donor ligand)

Martin Börner,[a, b] Jennifer Klose,[a] Matias E. Gutierrez Suburu,[c, d] Cristian A. Strassert,[c, d] Fangshun Yang,[b] Kirill Yu. Monakhov,[b] Bernd Abel,[b, e] and Berthold Kersting*[a]

Abstract: The synthesis, structure, magnetic, and photophysical properties of two dinuclear, luminescent, mixed-ligand $[Cr^{III}_2L(O_2CR)]^{3+}$ complexes (R = CH_3 (**1**), Ph (**2**)) of a 24-membered binucleating hexa-aza-dithiophenolate macrocycle $(L)^{2-}$ are presented. X-ray crystallographic analysis reveals an edge-sharing bioctahedral $N_3Cr(\mu\text{-}SR)_2(\mu_{1,3}\text{-}O_2CR)CrN_3$ core structure with $\mu_{1,3}$-bridging carboxylate groups. A ferromagnetic superexchange interaction between the electron spins of the Cr^{3+} ions leads to a high-spin ($S = 3$) ground state. The coupling constants ($J = +24.2(1)$ cm^{-1} (**1**), $+34.8(4)$ cm^{-1} (**2**), $H = -2JS_1S_2$) are significantly larger than in related *bis*-μ-alkoxido-μ-carboxylato structures. DFT calculations performed on both complexes reproduce both the sign and strength of the exchange interactions found experimentally. Frozen methanol-dichloromethane 1:1 solutions of **1** and **2** luminesce at 750 nm when excited into the ^{4}LMCT state on the $^4A_2 \rightarrow {}^2T_1$ (ν_2) bands ($\lambda_{exc} = 405$ nm). The absolute quantum yields (Φ_L) for **1** and **2** were found to be strongly temperature dependent. At 77 K in frozen MeOH/CH_2Cl_2 glasses, $\Phi_L = 0.44 \pm 0.02$ (for **1**), $\Phi_L = 0.45 \pm 0.02$ (for **2**).

Introduction

Polynuclear chromium(III) complexes have unique magnetic[1] and optical properties[2] and the number of reported complexes with well-defined nuclearity is growing steadily.[3–13] A particularly large number of dinuclear mixed-ligand chromium(III) complexes have been prepared[14] in order to investigate the interplay between electron exchange and photoinduced properties.[15] With respect to d-d spectra, for example, simultaneous pair excitations, which are absent in the spectra of monomeric complexes,[16–19] become possible due to exchange interactions.[20] The intensity enhancement of transitions involving ligand-field states (LF) has also been a well-known effect of binuclear interactions in chromium(III) dimers. The vast majority of exchange-coupled chromium(III) complexes employ bridging oxido,[21–23] hydroxido,[24,25] alkoxido,[26] halido,[27] and carboxylato[28] ligands. Recently, a number of semiquinoid radical bridging ligands have been used to obtain large magnetic exchange interactions between Cr^{III} centers.[29–31] The magnetic exchange interactions in the majority of these dimers is antiferromagnetic in nature.[32,33] Only few ferromagnetically coupled chromium(III) complexes have been reported.[34–36] Recently, a method for the targeted construction of ferromagnetically coupled chromium(III) complexes was reported.[37] Compounds with a $Cr^{III}(\mu\text{-}OR)_2(\mu_{1,3}\text{-carboxylato})Cr^{III}$ core structure have been prepared with ferromagnetic coupling constants in the range $+0.37 < J < +8.02$ cm^{-1} ($H = -2JS_1S_2$).

We have been interested in the coordination chemistry of dinuclear mixed-ligand complexes supported by the macrocyclic hexa-amine dithiophenolato ligand H_2L (Figure 1). The doubly deprotonated form, L^{2-}, is an effective dinucleating ligand that readily forms bioctahedral complexes of the type $[M_2L(\mu\text{-}L')]^+$ with various first-row transition metal ions ($M = Mn^{2+}$, Fe^{2+}, Co^{2+}, Co^{3+}, Ni^{2+}, Figure 1).[38] Several co-ligands such as $L' = Cl^-$, OH^-,[39] HS^-,[40] and RCO_2^-,[41–46] to name just a few, can be accommodated between the divalent metal ions. Complexes of this kind offer the opportunity to investigate intramolecular magnetic super-exchange interaction as a function of the electronic configuration of the metal ions and

[a] Dr. M. Börner, Dr. J. Klose, Prof. Dr. B. Kersting
Institut für Anorganische Chemie
Universität Leipzig
Johannisallee 29, 04103 Leipzig (Germany)
E-mail: b.kersting@uni-leipzig.de
[b] Dr. M. Börner, F. Yang, Dr. K. Y. Monakhov, Prof. Dr. B. Abel
Leibniz Institut für Oberflächenmodifizierung
Permoserstraße 15, 04318 Leipzig (Germany)
[c] M. E. Gutierrez Suburu, Prof. C. A. Strassert
Institut für Anorganische und Analytische Chemie
CiMIC, SoN
Westfälische Wilhelms-Universität Münster
Corrensstraße 28/30, 48149 Münster (Germany)
[d] M. E. Gutierrez Suburu, Prof. C. A. Strassert
CeNTech
Westfälische Wilhelms-Universität Münster
Heisenbergstraße 11, 48149 Münster (Germany)
[e] Prof. Dr. B. Abel
Wilhelm-Ostwald-Institut für Physikalische und Theoretische Chemie
Universität Leipzig
Linnéstrasse 2, 04103 Leipzig (Germany)

Supporting information for this article is available on the WWW under https://doi.org/10.1002/chem.202102079

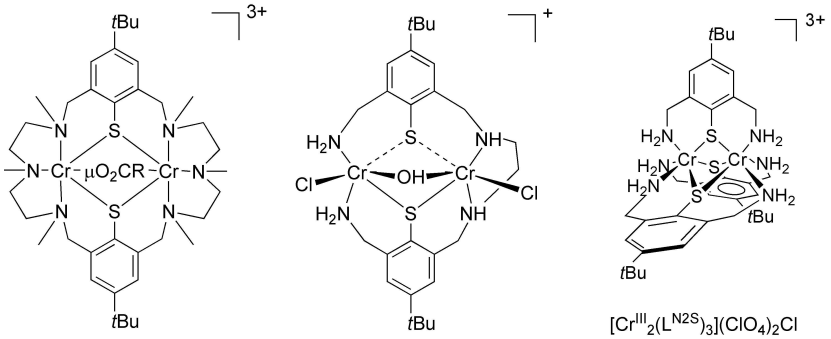

Figure 1. Dinuclear chromium(III) complexes supported by macrocyclic (H_2L, this work) and open chain amino-thiophenolato ligands (H_2L^{N4S2},[51] and HL^{N2S},[52]) respectively.

the type of the coligand. A magneto-structural correlation could already be derived for an isostructural series of $[M^{II}_2L(\mu\text{-}O_2CR)]^+$ complexes ($M^{II}=Mn^{2+}$, Fe^{2+}, Co^{2+}, and Ni^{2+}).[47] In these complexes, the magnitude and sign of the exchange interaction was found to depend primarily on the size of the M–S–M bridging angle. The ability of the amino-thiophenolato ligand H_2L to bind to trivalent metal ions is far less well documented. So far, only few Co^{III} complexes were reported.[48–50]

Some time ago, we reported dinuclear Cr^{III} complexes of open-chain amino-thiophenolato ligands H_2L^{N4S2} and HL^{N2S}, respectively (Figure 1).[51] From polarized optical absorption and emission spectroscopy, an antiferromagnetic exchange interaction was determined for $[Cr^{III}_2(L^{N2S})_3](ClO_4)_2Cl$.[52] Given the ferromagnetic exchange interactions found in compounds with a $Cr^{III}(\mu\text{-}OR)_2(\mu_{1,3}\text{-carboxylato})Cr^{III}$ core structure,[37] it was of interest to study analogous complexes with dithiolato-bridged Cr^{III} centres. The macrocyclic ligand with its N_6S_2 donor set was considered suitable for the synthesis of such target structures. Metalation of polydentate ligands with labile Cr^{II} sources followed by oxidation with aerial oxygen has turned out to be a successful strategy for the synthesis of inert Cr^{III} complexes.[53] By adopting this procedure, we have now been successful in synthesizing the hitherto inaccessible $[Cr^{III}_2L(\mu\text{-carboxylato})]^{3+}$ complexes. Herein, we present their synthesis and detailed structural, electrochemical, magnetic, and spectroscopic characterization. As will be shown, **1** and **2** exhibit a $Cr^{III}(\mu\text{-}SR)_2(\mu_{1,3}\text{-carboxylato})Cr^{III}$ core structure reminiscent of the series of compounds recently reported by Rajaraman and Brechin.[37] Experimental coupling constants of $J=+24.2(2)\ cm^{-1}$ (**1**) and $+34.8(4)\ cm^{-1}$ (**2**) determined by variable temperature dependent susceptibility measurements demonstrate that moving from alkoxide to thiolato bridges can further enhance the ferromagnetic exchange interactions. The photophysical properties of these mixed-ligand chromium(III) complexes are also reported and compared with their mononuclear counterparts.

Results and Discussion

The new chromium(III) complexes **1** and **2** were prepared according to Scheme 1. The hydrochloride salt of the macrocyclic supporting ligand was allowed to react with $CrCl_2$ and the corresponding triethylammonium carboxylate (1:2:1 ratio) in MeOH for 12 h at room temperature, followed by oxidation with aerial oxygen to provide brown-red solutions containing the cations of the title compounds $[Cr^{III}_2L(\mu\text{-}O_2CR)]^{3+}$ (R = Me, Ph). Upon addition of $LiClO_4$, the purple to reddish-brown, air-stable perchlorate salts $[Cr^{III}_2L(\mu\text{-}O_2CR)](ClO_4)_3$ (R = Me (**1**), Ph (**2**)) precipitated in 64–69% yield. The perchlorate salts exhibit good solubility in acetonitrile, methanol, and halogenated hydrocarbons, but they are only sparingly soluble in ethanol and virtually insoluble in water. The complexes gave satisfactory elemental analyses, and their formulation as dinuclear, mixed-ligand complexes was confirmed by electrospray ionization mass spectrometry (ESI-MS), IR-spectroscopy, cyclic voltammetry (CV), and single-crystal X-ray diffractometric analysis.

The ESI-MS spectra (*+ve* mode) of dilute (10^{-3} M) solutions of **1** and **2** in MeCN show three predominant peaks (Figure S1,2

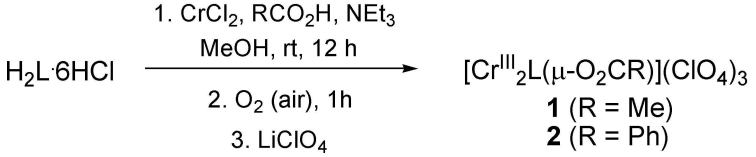

Scheme 1. Synthesis of **1** and **2**.

Supporting Information), attributable to the parent $[Cr_2L(\mu\text{-}O_2CR)]^{3+}$ trications (*m/z* = 277.1 (**1**), 297.8 (**2**)), and the perchlorate adducts $[Cr_2L(\mu\text{-}O_2CR)](ClO_4)^{2+}$ (*m/z* = 465.2 (**1**), 496.2 (**2**)) and $[Cr_2L(\mu\text{-}O_2CR)](ClO_4)_2^{+}$ (*m/z* = 1029.5 (**1**), 1091.27 (**2**)), respectively. These results suggest that the Cr^{III} compounds exist as discrete dinuclear species in solution. The infrared spectra of **1** and **2** display the bands expected for the macrocyclic ligand $(L)^{2-}$, counterions, and carboxylato coligands (Figure S3,4). The ClO_4^- ions give rise to two characteristic bands at 1100 cm^{-1} and 624 cm^{-1} typical for this counterion.[54] Each spectrum displays two further strong absorptions (1525 cm^{-1}, 1452 cm^{-1} (**1**); 1523 cm^{-1}, 1410 cm^{-1} (**2**)), which are tentatively assigned to the asymmetric ($\nu_{as}(RCO_2^-)$) and symmetric stretching vibrations ($\nu_s(RCO_2^-)$) of the $\mu_{1,3}$-bridging carboxylato ligands.[55] The carboxylate stretching frequencies compare well with those of the analogous Co^{III} complexes (i.e. $[Co^{III}_2L(\mu\text{-}OAc)](ClO_4)_3$: $\nu_{as}(RCO_2^-) = 1525\ cm^{-1}$, $\nu_s(RCO_2^-) = 1427\ cm^{-1}$).[48]

Cyclic voltammetry

Cyclic voltammetry was performed in order to determine the redox properties of **1** and **2**. Cyclic voltammograms (CV) were recorded in CH_3CN solution using $[Bu_4N][PF_6]$ as the supporting electrolyte. The formal potentials are referenced versus ferrocenium/ferrocene ($Fe(Cp)_2^+/Fe(Cp)_2$) used as an internal standard. The CV of **1** (Figure 2) displays two reversible redox waves at quite negative potentials, $E^{0'}_{1/2} = -1.39$ V ($\Delta E_p = 76$ mV) and $E^{0'}_{1/2} = -0.85$ V ($\Delta E_p = 69$ mV) vs. $Fe(Cp)_2^+/Fe(Cp)_2$. The CV of **2** is similar to that of **1**, showing two redox waves at $E^{0'}_{1/2} = -1.33$ V ($\Delta E_p = 71$ mV) and $E^{0'}_{1/2} = -0.81$ V ($\Delta E_p = 71$ mV).

Given the presence of two redox-active Cr^{III} ions in complexes **1** and **2**, the redox wave at −0.85 V is readily assigned to a metal-centered one-electron reduction (Eq. (1)). The resultant $Cr^{III}Cr^{II}$ species undergoes another reduction step at ca. 0.55 V more negative potentials to produce the parent $Cr^{II}Cr^{II}$ complexes (Eq. (2)). The electrochemical response of **1** resembles that of the analogous cobalt(III) complex. The diamagnetic Co^{III} complexes, however, are reduced at much more anodic potentials ($E^{0'}_{1/2}$ ($Co^{III}Co^{II}/Co^{II}Co^{II}$): −0.19 V; $E^{0'}_{1/2}$ ($Co^{III}Co^{III}/Co^{III}Co^{II}$): +0.20 V).[48] The anodic potential regime is featureless up to +2 V vs. $FeCp_2^+/FeCp_2$ (full range not shown in Figure 2). In other words, the bridging thiophenolate head units in these inert chromium(III) complexes are redox inactive in this potential window.

$$[Cr^{III}_2L(\mu\text{-}O_2CR)]^{3+} + e^- \overset{E^{0'(1)}}{\rightleftharpoons} [Cr^{III}Cr^{II}L(\mu\text{-}O_2CR)]^{2+} \quad (1)$$

(oxidation level present in **1** and **2**)

$$[Cr^{III}Cr^{II}L(\mu\text{-}O_2CR)]^{2+} + e^- \overset{E^{0'(2)}}{\rightleftharpoons} [Cr^{II}_2L(\mu\text{-}O_2CR)]^{+} \quad (2)$$

Only few chromium(III) amine-thiolato complexes have been studied by cyclic voltammetry. Wieghardt and co-workers have reported a mononuclear, neutral $[Cr^{III}(tbm\text{-}tacn)]$ complex, where tbm-tacn represents a hexadentate trianionic ligand tris (4-*tert*-butyl-2-mercaptobenzyl)-1,4,7-triazacyclononane providing an N_3S_3 donor set.[56] The Cr^{II} oxidation level of this complex is not accessible down to −1.86 V vs. $Fe(Cp)_2^+/Fe(Cp)_2$. Related Cr^{III} hexamine complexes are reduced at −1.61 to −1.76 V vs. $Fe(Cp)_2^+/Fe(Cp)_2$.[57] Complexes **1** and **2** with bridging thiolato units are obviously much easier to reduce. This may be attributed to the differences in the overall charge of the complexes and/or to differences in the metal-ligand bonding interactions. The properties of bridging thiolato ligands have been compared with those of thioethers.[58] Thioethers are known to delocalize d electrons into π acceptor orbitals thereby stabilizing metal ions in low oxidation states.[59] Our observations are in agreement with this notion.

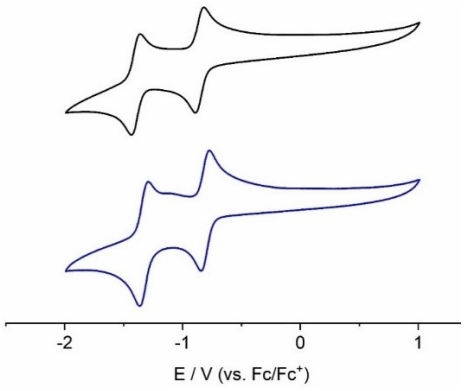

Figure 2. Cyclic voltammograms of **1** (top) and **2** (bottom, blue curve) in acetonitrile at ambient temperature (Pt disk working electrode, Pt wire counter electrode, Ag/AgCl reference electrode, 0.1 M NBu_4PF_6 supporting electrolyte, scan rate 100 mV/s).

Molecular structure from X-ray diffractometric analysis of single crystals

Single crystals of $\mathbf{1}\cdot 2H_2O$ were obtained from MeCN/EtOH. Table 1 lists selected bond lengths and angles. The crystal structure of $\mathbf{1}\cdot 2H_2O$ is composed of well-separated $[Cr_2L(\mu\text{-}O_2CMe)]^{3+}$ trications (Figure 3), perchlorate anions, and water solvate molecules. The acetate ion bridges the Cr^{III} centers in a symmetrical fashion at a Cr···Cr distance of 3.545 Å, ruling out the presence of direct metal–metal bonds.[60] The closest intermolecular Cr···Cr distance is much longer (9.276 Å).

Both Cr^{III} atoms are coordinated by three N and two S atoms from the macrocycle and one acetate O atom in a severely distorted pseudo-octahedral fashion. The metal ligand bond angles deviate by as much as 13° from the ideal octahedral values. The average Cr–N, Cr–O, and Cr–S bond lengths at 2.166 Å, 1.951 Å, and 2.447 Å, respectively, show no unusual features and compare well with those of other octahedral Cr^{III} complexes with mixed S, N, O coordination.[61–66] It should be noted that the Cr-S–Cr angles in **1** are much more obtuse than in $[Cr^{III}_2(L^{N2S})_3]^{3+}$ (92.83° versus 77.7°).[52] This parameter has

Table 1. Experimental and DFT calculated bond lengths [Å] and angles [°] for **1**·2H_2O and **2**·*x*MeCN (*x* ~4.5).[a]

	1·2H_2O	$\mathbf{1}_{calcd}$	**2**·*x*MeCN (*x* ~4.5)[b]	$\mathbf{2}_{calcd}$[c]
Cr(1)-O(1)	1.948(2)	1.958	1.964(3) [1.963(3)]	1.934
Cr(1)-N(1)	2.168(2)	2.249	2.206(3) [2.155(3)]	2.199
Cr(1)-N(2)	2.120(2)	2.173	2.132(4) [2.132(3)]	2.168
Cr(1)-N(3)	2.206(2)	2.173	2.162(3) [2.214(3)]	2.249
Cr(1)-S(1)	2.4302(9)	2.470	2.439(1) [2.404(1)]	2.426
Cr(1)-S(2)	2.4671(8)	2.426	2.398(1) [2.440(1)]	2.433
Cr(2)-O(2)	1.953(2)	1.953	1.954(3) [1.960(3)]	1.952
Cr(2)-N(4)	2.203(2)	2.201	2.166(4) [2.214(4)]	2.242
Cr(2)-N(5)	2.119(2)	2.175	2.129(3) [2.131(4)]	2.174
Cr(2)-N(6)	2.180(2)	2.248	2.213(4) [2.153(4)]	2.198
Cr(2)-S(1)	2.4356(8)	2.460	2.434(1) [2.407(1)]	2.419
Cr(2)-S(2)	2.4560(9)	2.435	2.400(1) [2.446(1)]	2.490
cis-L–Cr-L	77.11(3)–99.31(8)	76.7–102.8	77.34(4)–100.95(13) [77.16(4)–100.15(13)]	76.8–101.9
trans-L–Cr-L	167.17(6)–169.58(6)	166.4–167.5	167.65(10)–169.55(13) [167.91(10)–169.16(13)]	166.4–167.8
S(1)-Cr(1)-S(2)	77.11(3)	76.7	77.34(4) [77.32(4)]	76.8
S(1)-Cr(2)-S(2)	77.22(2)	76.7	77.39(4) [77.16(4)]	76.8
Cr(1)-S(1)-Cr(2)	93.53(3)	92.0	92.16(4) [93.90(4)]	93.8
Cr(1)-S(2)-Cr(2)	92.12(3)	93.7	94.01(4) [92.04(4)]	90.7

[a] The coordinates of the optimized structures of **1** and **2** are tabulated in Tables S6 and S7. [b] The asymmetric unit of **2**·*x*MeCN (*x* ~4.5) comprises two chemically identical but crystallographically independent molecules A and B. The values in square brackets refer to molecule B. [c] Coordinates of cation A were used as input for the DFT calculations.

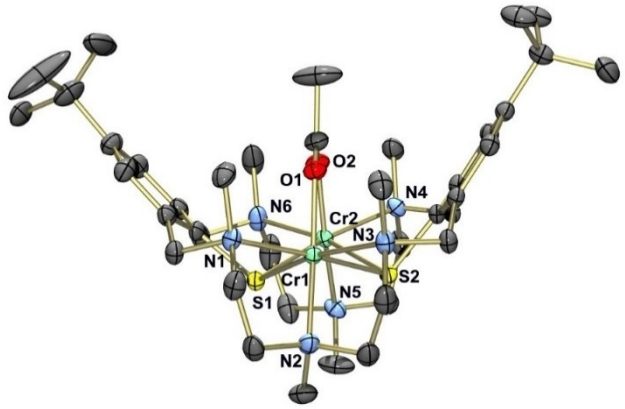

Figure 3. Structure of the $[Cr^{III}_2L(\mu_{1,3}\text{-}O_2CMe)]^{3+}$ cation in crystals of **1**·2H_2O. Thermal ellipsoids are drawn at the 50% probability level. Only one orientation of a disordered *tert*-butyl group is shown. Hydrogen atoms are omitted for reasons of clarity.

turned out to be an important factor in terms of the sign and magnitude of the magnetic exchange interactions. Complexes with related $Cr^{III}(OR)_2(\mu\text{-}O_2CR)Cr^{III}$ core structures are ferromagnetically coupled. $[Cr_2(Me\text{-}deaH)_2(O_2CR)Cl_2]^+$ (Me-deaH = 2-(dimethylamino)-ethanol) is a recent example.[26,37] We note that the Cr–O–Cr angles in this alkoxido-bridged complex are significantly larger than in **1**. This parameter is therefore discussed again in the next section. Crystals of the benzoato-bridged complex **2**·$MeCN_x$ (*x* ~4.5) were also grown from MeCN/EtOH. The $[Cr_2L(\mu\text{-}O_2CPh)]^{3+}$ cation is isostructural with that in **1** (Figure S5). The corresponding bond lengths and angles are virtually the same. Selected bond lengths and angles for **1** and **2** are compiled in Table 1. The DFT optimized geometries of **1** and **2** at the B3LYP/def2-TZVPP level of theory agree reasonably well with the experimental data (Table 1).

Magnetic properties

Complexes **1**·2H_2O and **2**·*x*MeCN (*x* ~4.5) were further studied by variable-temperature magnetic susceptibility measurements in order to determine the magnetic exchange interactions. The susceptibility data have been measured for powdered solid samples between 2.0 and 300 K using a MPMS 7XL SQUID magnetometer in applied external magnetic fields *B* of 0.1 T and 0.5 T. In no case was any significant field dependence of the magnetic data observed. Plots of the temperature dependence of the effective magnetic moment μ_{eff} (per binuclear complex) are shown in Figure 4.

For complex **1**, the effective magnetic moment μ_{eff} (per dinuclear complex) at 300 K amounts to 6.09 μ_B, a value somewhat higher than that expected for two non-interacting $S = 3/2$ ions with $g = 2.0$ (5.48 μ_B). Upon decreasing temperature, the magnetic moment increases steadily to a maximum value of 6.84 μ_B at 30 K. On further cooling μ_{eff} decreases to 6.53 μ_B at 2 K. Complex **2** showed a very similar behavior. The effective magnetic moment increases gradually from 6.37 μ_B at 295 K to 6.84 μ_B at 40 K, and then decreases to 6.50 μ_B at 2 K. This behavior suggests that the electron spins of the two Cr^{III} ($S_{1,2} = 3/2$) ions are coupled by an intramolecular ferromagnetic (FM) exchange interaction to give an $S = 3$ high-spin ground state. The $S = 3$ ground state is further confirmed by variable-temperature variable-field magnetisation measurements, performed in the $B = 0.5$–7 T field ranges at 2 K (Figure S6, S7). The high field saturation moment $M_{sat} = gS\mu_B$ ($g = 2$) is close to 6 μ_B per dinuclear complex as expected for a $S = 3$ high-spin ground state.

The susceptibility data of **1** and **2** were fitted by a full-matrix diagonalization approach applying the appropriate isotropic Heisenberg-Dirac-van Vleck model (Eq. (3)) in order to analyze

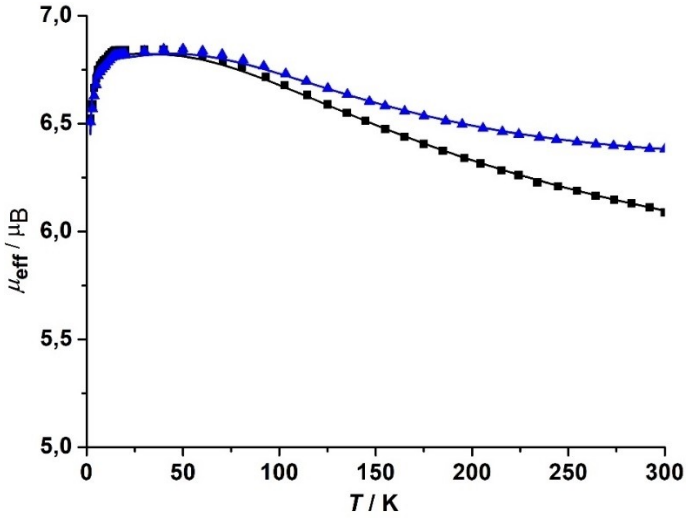

Figure 4. Temperature dependence of μ_{eff} versus T for compounds **1**·2H$_2$O (■) and **2**·xMeCN (x ~4.5) (▲) (B = 0.5 T). The full lines represent the best theoretical fits to equation 3. Fit parameters are given in the text.

the magnitude of the exchange interactions.[67] The Hamiltonian in Equation (3) includes two terms to account for exchange coupling ($-2JS_1S_2$) and Zeeman interactions. An intermolecular exchange interaction parameter zJ (mean-field approximation) between the Cr(III) complexes was also considered to account for the drop in the χT product at low temperatures. The g values are assumed to be identical for the two Cr^{III} ions. Reasonable fits of the experimental data were possible, yielding $J = +24.2(2)$ cm^{-1}, $g = 1.98$, and $zJ = -0.0053(3)$ cm^{-1} for complex **1** and $J = +34.8(4)$ cm^{-1}, $g = 1.98$ and $zJ = -0.0057(5)$ cm^{-1} for complex **2**. The small values for the exchange interaction parameter is well in line with the rather large intermolecular separation of the chromium(III) complexes (>9 Å).[68] The experimental J values agree also reasonably well with those obtained by broken-symmetry density functional theory (DFT) calculations (B3LYP/def2-TZVPP level of theory) for **1** ($J_{calc} = +31.07$ cm^{-1}) and **2** ($J_{calc} = +29.81$ cm^{-1}, Table S2). According to the Landé formula (Eq. (4)), the septet-quintet, quintet-triplet, and tiplet-singlet splitting in the ground state of **1** amount to $\Delta E = 145.2$ cm^{-1} ($6\times J$), 96.8 cm^{-1} ($4\times J$), and 48.4 cm^{-1} ($2\times J$), respectively, to give a total energy span of 290.4 cm^{-1} for the spin ladder.[72]

$$\hat{H} = -2J\hat{S}_1\hat{S}_2 + \sum_{i=1}^{2}[g_i\mu_B S_{i\tau}B_\tau] \ (\tau = x, y, z) \tag{3}$$

$$E(S) = -J[S(S+1)\text{-}S_1(S_1+1)\text{-}S_2(S_2+1)] \tag{4}$$

The experimental J values for **1** and **2** are the largest yet reported for ferromagnetically coupled chromium(III) complexes and surpass the coupling in the related bis-μ-alkoxido-μ-carboxylato bridged Cr^{III} dimers by a factor of 3.[26,37] This finding is consistent with the observation that thiolato bridges can more efficiently propagate magnetic exchange interactions.[69,70] The ferromagnetic exchange interactions found for **1** and **2** are also in contrast to the antiferromagnetic (AFM) exchange interactions present in $[Cr_2(L^{N2S})_3]^{3+}$ ($J = -39$ cm^{-1} ($H = -2JS_1S_2$)). It is tempting to attribute the different magnetic properties to structural differences in the bridging region, given that $[Cr_2(L^{N2S})_3]^{3+}$ exhibits an face-sharing bioctahedral geometry, while **1** and **2** reveal an edge-sharing core geometry. The Cr–S–Cr angle widen significantly from 77.7° in $[Cr_2(L^{N2S})_3]^{3+}$ to 92.8° in **1** and 93.0° in **2**. The increase of the Cr–S–Cr bond angle is the most significant structural difference, and, hence, may account for the change of the coupling type.

It should be mentioned that the mechanisms and parameters that govern the exchange interactions in chromium(III) dimers bridged by oxido, hydroxido, or alkoxido ligands are qualitatively quite well understood.[71] For doubly and triply bridged dimers of the type [Cr^{III}(μ-OR)$_2$Cr^{III}][25] and [Cr^{III}(μ-OR)$_2$(μ-O$_2$CR)Cr^{III}] (R = H or alkyl),[37] respectively, the magnitude and sign of the magnetic interaction has been shown to correlate with several structural parameters, as for instance the Cr–O–Cr bridging angle, the Cr–O bond length, and the dihedral angle spanned between the bridging Cr_2O_2 plane and the OR vector. Magnetic susceptibility measurements and accompanying DFT calculations shows that the bridging Cr–O–Cr angle has the largest effect on the coupling type. Thus, strong AFM coupling was observed for small angles (83–98°) while larger angles (98–108°) yield a weaker FM behaviour.

In order to shed more light on the pathways, by which the interaction between the paramagnetic Cr(III) sites is mediated, we have investigated direct and differential overlap of the "corresponding orbital pairs" from the BS-DFT solutions for **1** and **2**, as done for other triply bridged Cr(III) complexes.[72,73] The results of the corresponding orbital transformations are shown in Figures S8 and S9. The small overlap integrals for the corresponding orbital pairs (0.033, 0.022, 0.011 for the orbitals 218, 219 and 220 (for **1**), 0.035, 0.031, 0.011 for orbitals 234, 235, and 236 (for **2**), respectively), suggest that direct metal-

metal through-space interactions are not significant in the present complexes. In triply-hydroxido-bridged chromium(III) dimers, which feature direct Cr···Cr (d_z^2-d_z^2) interactions, the overlap integrals are much larger. For $[L_2Cr^{III}_2(\mu\text{-}OH)_3]^{+3}$ (L = N,N′,N″-trimethyl-1,4,7-triazacyclononane, for example, an *S* value of 0.224 has been calculated for the direct interaction of the magnetic d_z^2 orbital. In view of the much smaller Cr···Cr distance (2.642(2) Å)[74] and the different alignment of orbitals, this is not surprising. The BS-DFT analysis further reveals that the three magnetic orbitals in **1** and **2** resemble the chromium d_{xy}, d_{xz}, and d_{yz} orbitals. In the case of these orbitals pairs, overlap occurs over the bridging ligands.[75] The calculated Mulliken α spin density at the two chromium atoms at ~3.29 is greater than 3.0 electrons, indicative of the presence of a spin polarisation mechanism that leads to the larger than expected spin density values. The spin density plot reveals a cube shaped spin density on the metal atoms resulting from the t_{2g}^3 configuration of the Cr^{3+} ions (Figure 5). The spin densities on the terminal nitrogen atoms show only spin polarisation. The spin densities on the bridging carboxylato and thiophenolato ligands feature both a mixture of spin polarisation and spin delocalisation (Table S2, S3).

Broken symmetry density functional theory calculations on truncated model complexes **1′** and **2′** (with the carboxylato-bridges removed) have also been performed to study the individual contributions of the carboxylate ligands and thiolato-bridges to the overall magnetic behaviour. This approach has previously proven to be a powerful tool to unravel the contributions of the individual bridges in Ni complexes supported by $(L)^{2-}$.[76,77] These results imply that a dominant "ferromagnetic" contribution (39.85 cm^{-1} (**1**), 41.13 cm^{-1} (**2**), Table S3) through the bridging thiolato ligands is counter-balanced by an antiferromagnetic interaction through the carboxylates. Such an orbital countercomplementary effect was also observed for the series of carboxylato-bridged chromium (III) complexes reported by Rajaraman and Brechin.[37] Our observations suggest that a similar effect exists for the present compounds.

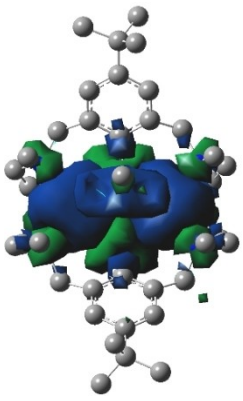

Figure 5. DFT calculated spin density plot for complex **1** (B3LYP/def2-TZVPP level of theory, isosurface value 0.005 a.u., hydrogens omitted for clarity).

Spectroscopic and photophysical properties

The spectroscopic properties of the Cr^{III} complexes were further studied by UV-vis absorption as well as photoluminescence excitation and emission spectroscopy. The UV-vis absorption spectrum of complex **1** in MeCN is representative (Figure 6) and will be discussed. The spectral data is summarized in Table 2. The near UV region is dominated by two intense absorption bands at 210 nm and 247 nm; a shoulder at ~275 nm is also clearly discernible. All features are attributed to spin-allowed transitions into π-π* states of the macrocyclic amino-thiophenolato ligand. Intense bands in the 210–300 nm range are typical for metal complexes containing thiophenolato ligands.[56] The diamagnetic $[Zn_2L(\mu\text{-}OAc)]^+$ complex, for example, reveals intense transitions into π-π* configured states at similar wavelengths, namely λ_{max} = 261 nm (ε = 13740 $M^{-1}cm^{-1}$) and 288 nm (ε = 24464 $M^{-1}cm^{-1}$).[78]

The spectrum of **1** reveals another intense absorption maximum at 363 nm (ε = 2660 $M^{-1}cm^{-1}$), which is assigned to a transition into a thiophenolate-to-Cr^{III} charge transfer state. Analogous transitions into ligand-to-metal charge transfer (LMCT) configurations for $[Cr_2(L^{N2S})_3]^{3+}$ and $[Cr_2(L^{N4S2})(\mu\text{-}OH)(Cl)_2]^+$ are observed at similar wavelengths (317 nm, 352 nm, Table 2). The $[Zn^{II}_2L(\mu\text{-}OAc)]^+$ complex, on the other hand, does not absorb in this region, providing strong support for the LMCT nature of the states related to these intense absorption bands.[78] The finding that the ^{4}LMCT configurations can feed the emissive $^2T_1$ $^4A_2/^2E$ $^4A_2$ excited state of **1** and **2** (see excitation spectra discussed below) suggests that these complexes may also be interesting to investigate as sensitizers based on earth-abundant metal ions[79,80] or as acceptors in supramolecular architectures.[81–84]

The visible region of the spectrum of **1** reveals a shoulder on the low-energy tail of the LMCT-related band at ~417 nm and a well-defined absorption band peaking at around 571 nm

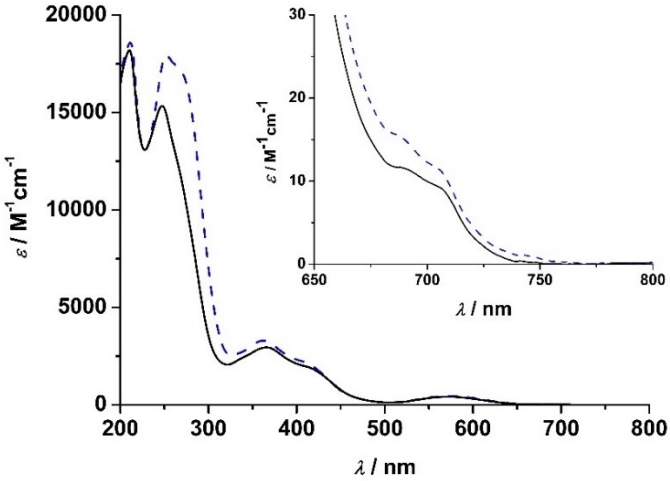

Figure 6. UV-vis absorption spectra of **1** (black line) and **2** (blue dashed line) in fluid MeCN solution at 295 K ($c = 10^{-4}$ M). The inset shows the region of the spin-forbidden $^4A_2 \rightarrow {}^2T_1$, ^2E transitions in the 650 to 750 nm range (note the different scales).

Table 2. Comparison of spectroscopic properties of six-coordinated chromium(III) complexes containing N, O, and S donor ligands (transitions into ligand field states in *O* notation), λ_{max}/nm (ε/$M^{-1}cm^{-1}$).

Compound	Coord. Environ.	π-π*	LMCT	ν_2	ν_1	$^4A_2\rightarrow{}^2T_1$, ^2E	Ref
1[a]	N_3S_2O	210 (18189) 247 (15389) 270 (11233)	366 (2950)	417 sh (1876)	572 (414)	690 sh (< 12) 707 sh (< 8) 740 sh (< 2)	this work
1[g]	N_3S_2O	211 253 275	374	410	577	689 sh 706 sh –	this work
2[a]	N_3S_2O	211 (18691) 252 (17979) 271 (17028)	363 (3324)	412 sh (2160)	573 (456)	689 sh (< 15) 706 sh (< 11 740 sh (< 2)	this work
2[g]	N_3S_2O	255 272	372	414	572	692 sh 704 sh	this work
$[Cr_2(L^{N2S})_3]^{3+}$, [a]	N_3S_3		317 (6920)	410 sh	533 (275)	n.o.	[52]
$[Cr_2(L^{N2S})_3]^{3+}$, [b]	N_3S_3	250	285-357	420	526		[52]
$[Cr_2(L^{N2S})_3]^{3+}$, [c]	N_3S_3					655-750	[52]
$[Cr_2(L^{N4S2})(\mu\text{-}OH)(Cl)_2]^{+}$, [a]	N_2S_2OCl		352 (5500)	433 sh	592 (436)	n.o.	[51]
$[Cr_2(L^{N4S2})(\mu\text{-}Cl)(Cl)_2]^{+}$, [a]	N_2S_2OCl		354 (5890)	445 sh	594 (380)	n.o.	[51]
$[Cr(en)_3]^{3+}$, [d]	6×N		–	351 (70)	457 (86)	–	[57]
$[Cr(H_2O)_6]^{3+}$	6×O		–	426	575	666	[87]
$[Cr(bmts)_2]^{3+}$, [a,e]	6×S		–	436	636	ca. 689	[87]
[Cr(tbm-tacn)], [f]	N_3S_3		–	460	591	–	[56]

[a] MeCN, 10^{-4} M, 295 K. [b] Glycerol glass, 20 K. [c] Single-crystal absorption spectral data. [d] en = ethylenediamine. [e] bmts = bis(3-methylthiopropyl) sulfide. [f] tbm-tacn = *tris*(4-*tert*-butyl-2-mercaptobenzyl)-1,4,7-triazacyclononane. [g] Samples were optically diluted with $BaSO_4$ (~95 wt%).

(ε = 414 $M^{-1}cm^{-1}$). These two features are tentatively assigned to the spin-allowed $^4A_2\rightarrow{}^4T_1$ (ν_2) and $^4A_2\rightarrow{}^4T_2$ (ν_1) transitions involving ligand-field-related states (symmetry labels according to *O* notation),[85] respectively. The intensity of these metal-centred transitions is relatively high, most likely due to ligand-imposed deviations from the octahedral symmetry. Metal centred transitions in dinuclear complexes are also referred to as single excitations, since formally only one of the two metal ions of the dinuclear core is excited.[2,86] In this notation, the spin-allowed ν_2 and ν_1 transitions would be referred to as $^4A_2{}^4A_2\rightarrow{}^4T_1{}^4A_2$ and $^4A_2{}^4A_2\rightarrow{}^4T_2{}^4A_2$, respectively.

Few dinuclear Cr^{III} complexes coordinated by amino-thiophenolato ligands have been investigated by UV-vis spectroscopy. Weak, spin-allowed ν_2 and ν_1 transitions involving ligand-field-related states for $[Cr_2(L^{N2S})_3]^{3+}$, $[Cr_2(L^{N4S2})(\mu\text{-}OH)(Cl)_2]^{+}$ and $[Cr_2(L^{N4S2})(\mu\text{-}Cl)(Cl)_2]^{+}$ are observed at similar energies (c.f. Table 2), with ν_2 ranging from 420–445 nm and ν_1 in the 526–594 nm range, respectively.[51,52] In O_h symmetry, the metal-centered $^4A_{2g}\rightarrow{}^4T_{2g}$ (ν_1) transition allows a direct determination of the ligand field parameter *Dq* (or Δ_o). *Dq* is given by the relation $\nu_1 = 10D_q$.[87,88] Assuming that the assignments are correct and neglecting the lower site symmetry in the present cases, this yields *Dq* = 1748 cm^{-1} (Δ_o = 17482 cm^{-1}) for **1** and *Dq* = 1745 cm^{-1} (Δ_o = 17452 cm^{-1}) for **2**, respectively. The decrease in ligand field strength is consistent with the transition from the N_3S_3 coordination environment in $[Cr_2(L^{N2S})_3]^{3+}$ to a N_3S_2O coordination in **1** (and **2**), to a N_2S_2OCl environment in $[Cr_2(L^{N4S2})(\mu\text{-}OH)(Cl)_2]^{+}$. Stronger ligands that lie on the right hand side in the spectrochemical series (primary amine, thiolato) are replaced by weak field ligands that are further to the left (tertiary amine, carboxylato, halido, hydroxido) to produce the red-shifts in the absorption bands and the decrease in Δ_o.[89,90] The overall ligand field strength of L^{2-} is surprisingly low, comparable to a ligand field produced by six oxygen (aqua) donors. The *Dq* values of **1** and **2** may be compared with that of the $[Cr(H_2O)_6]^{3+}$ complex for which *Dq* = 1740 cm^{-1}.[87]

Closer inspection of the UV-vis spectra of **1** and **2** reveal several weak shoulders in the 670–750 nm range (inset Figure 6), which can be ascribed to components of the intra-configurational (t_2^3) $^4A_2\rightarrow{}^2T_1$ and $^4A_2\rightarrow{}^2E$ excitations resultant from the exchange interactions. The features are relatively intense for spin-forbidden transitions (ε_{max} ~2–12). Extinction coefficients for spin-forbidden transitions in monomeric chromium(III) complexes typically do not exceed 5 $M^{-1}cm^{-1}$.[16] This may be due to a relaxation of the spin selection rule by an electric-dipole exchange-mechanism as first proposed by Tanabe and co-workers, or to the low local symmetry about the Cr^{III} centers.[91,92] Similar observations were made for the $[Cr_2(L^{N2S})_3]^{3+}$ complex, which reveals several relatively intense bands in the 650–750 nm range attributed as $^4A_2{}^4A_2\rightarrow{}^2T_1{}^4A_2$ and $^4A_2{}^4A_2\rightarrow{}^2E{}^4A_2$ transitions.[52] The diffuse reflectance UV-vis spectra of the Cr^{3+} complexes **1** and **2** (~5 wt% dispersed in $BaSO_4$ pellet) are displayed in Figure S10. The spectra of the solid complexes are very similar to the solution spectra, displaying intense spin-allowed transitions into π-π*, LMCT and ligand field states at approximately the same energies (Table 2). The $^4A_2{}^4A_2\rightarrow{}^2E{}^4A_2$, $^2T_1{}^4A_2$ single excitations seen in the solution spectra are also observed in the diffuse reflectance spectra. A simplified energy level diagram for the chromium(III) complexes can be seen in Figure 7.

Complexes **1** and **2** were further characterized by steady state and time-resolved photoluminescence spectroscopy. Figure 8 displays the emission spectrum (λ_{ex} = 405 nm) of complex **1** at 77 K in a frozen CH_2Cl_2/MeOH glassy matrix which is representative (see Figure S11 for the corresponding spectrum

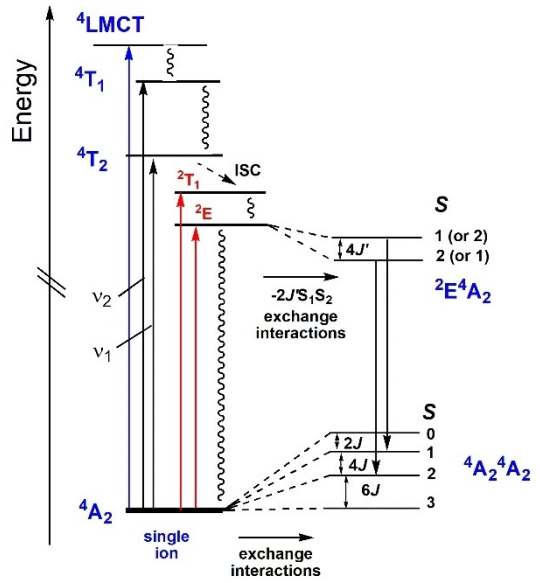

Figure 7. Qualitative energy level diagram of the ground and singly excited states for the chromium(III) complexes **1** and **2** showing electronic transitions and possible energy transfer pathways. Energy levels are not drawn to scale. The single ion energy levels (in the absence of exchange interactions) are shown on the left (levels assigned in O notation). Energy is absorbed by the LMCT and ligand field (ν_1, ν_2) transitions to populate the $^4T_2{}^4A_2$ state. Intersystem crossing (ISC) then leads to population of the emissive $^2T_1{}^4A_2$ and/or $^2E^4A_2$ states. Non-radiative (wavy lines) pathways lead to quenching of excited states. Right: The spin states (S) resulting from exchange interactions are only shown for the lowest excited $^2E^4A_2$ and the $^4A_2{}^4A_2$ ground state. The sign and size of the exchange interaction (J') in the excited $^2E^4A_2$ state could not yet be determined. Two of several allowed emission bands (expected to get intensity from the single-ion mechanism and the exchange interactions) are drawn (Boltzmann population not considered). This level of approximation implies that the ^2E and $^2T_1$ states are degenerate, which is clearly not the case in these complexes.

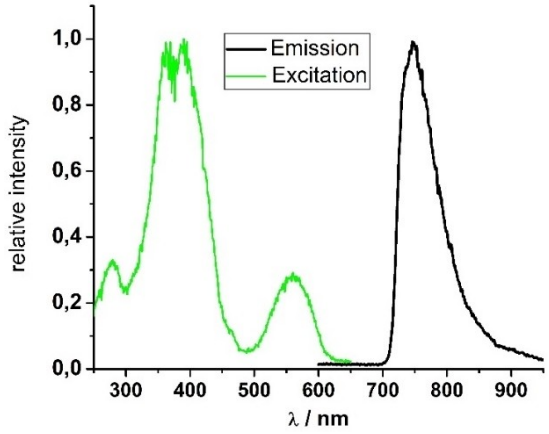

Figure 8. Excitation ($\lambda_{obs}=750$ nm, green curve) and emission spectra ($\lambda_{exc}=405$ nm, black line) of complex **1** at 77 K in a frozen CH_2Cl_2/MeOH 1:1 glassy matrix.

of **2**). The emission maximum at ~750 nm obtained upon excitation at the absorption band corresponding to the $^4A_2{}^4A_2 \rightarrow {}^4T_1{}^4A_2$ transition ($\lambda_{exc}=405$ nm) is attributed to radiative relaxation from the excited $^2E^4A_2$ state. A $^2E^4A_2$ energy ~1/750 nm is typical for chromium(III) complexes coordinated by sulfur-based donor ligands. Thiolato ligands are known to decrease electron repulsion by delocalization of d electrons into antibonding π^* orbitals (nephelauxetic effect) thereby lowering the energy of the ^2E level.[16,93] The emission band is much broader (full width at half maximum height (FWHM) = 1140 cm^{-1}) than typically seen in mononuclear complexes.[19] This may be due to the fact that several dimer levels of the excited and ground state are involved in the emission, as schematically illustrated in Figure 7. A similar behaviour has also been observed for the $[Cr_2(L^{N2S})_3]^{3+}$ complex.[52] The three bands at 750 nm, 735 nm, and 730 nm have been assigned to emissions from the $S=1$ and $S=2$ dimer levels of the $^2E^4A_2$ state. The excitation spectra of **1** and **2** monitored at 750 nm show strong absorption bands at 360 nm, 400 nm, and 560 nm (in good agreement with the absorption spectrum), suggesting that the excited ^{4}LMCT, $^4T_1{}^4A_2$, and $^4T_2{}^4A_2$ states all evolve to the emissive $^2E^4A_2$ doublet states as schematically illustrated in Figure 7.

Preliminary time resolved photoluminescence decay measurements of **1** and **2** in frozen CH_2Cl_2/MeOH glassy matrices at 77 K (Figure S12, S13) revealed upon excitation at 402.5 nm photoluminescence lifetimes τ_{obs} of 113.0 ± 0.8 µs (**1**) and 114.6 ± 0.9 µs (**2**), consistent with phosphorescence emission from the $^2E^4A_2$ excited state. The absolute photoluminescence quantum yields, measured with an integrating sphere, reach up to $\Phi_L = 0.45 \pm 0.02$ for **1** and $\Phi_L = 0.44 \pm 0.02$ for **2** at 77 K. Mononuclear chromium(III) complexes supported by saturated polyamine ligands or sulfur-based chelators exhibit similar luminescence lifetimes (τ_{obs} in the range 60–450 μs (CrN_6)[57,94–96] or 128–440 μs (CrS_6 complexes) at 77 K)[93] but with lower efficiency. The luminescence quantum yields do not exceed ~1 % for the $Cr^{III}N_6$[95,97] and ~5% for the $Cr^{III}S_6$ complexes.[93] The relaxation of the spin selection rule by an electric-dipole exchange-mechanism as also observed in the absorption spectra may account for the higher emission quantum yields for dinuclear **1** and **2**. The luminescence is quenched at higher temperatures in solution (Figure S14–S16).

Conclusions

The synthesis of two stable, discrete mixed-ligand chromium(III) complexes of the type $[Cr^{III}_2L(\mu\text{-}O_2CR)]^{3+}$ where L^{2-} represents a macrocyclic binucleating hexaamine-dithiophenolate ligand and O_2CR^- exogenous acetato (**1**) and benzoato coligands (**2**) has been highlighted. The synthesis involved metalation of the free macrocycle with labile Cr^{2+} ions in the presence of the respective carboxylato ligand followed by aerial oxidation of intermediate chromium(II) complexes. This route may thus well be generalised to synthesize other mixed-ligand chromium(III) complexes supported by the macrocyclic amino-thiophenolato ligand. Cyclic voltammetry on **1** and **2** revealed two reversible redox waves attributed to metal-centered one-electron reduction processes to afford the corresponding $[Cr^{II}Cr^{III}$-(L)(carboxylato)$]^{2+}$ and $[Cr^{II}Cr^{III}$(L)(carboxylato)$]^{+}$ cations at potentials of −0.85 and −1.35 V vs. $FeCp_2{}^+/FeCp_2$. X-ray

crystallographic analysis of single-crystals of **1** and **2** show that the carboxylato coligands are both installed as bridging units to generate central $[Cr^{III}(\mu\text{-}SR)_2(\mu\text{-}O_2CR)Cr^{III}]^{3+}$ core structures, which have not been described previously in dinuclear or dimeric chromium(III) complexes. The Cr(III) ions in complexes **1** and **2** are ferromagnetically coupled to produce a $S=3$ spin ground state, which stands in contrast to the $S=0$ ground state of the chromium(III) complex $[Cr^{III}_2(LN_2S)_3]^{3+}$ with a triply-thiophenolato-bridged $[Cr^{III}(\mu\text{-}SR)_3Cr^{III}]$ core. The magnetic coupling in **1** ($J=24.2(1)\ cm^{-1}$) and **2** ($J=+34.8(4)\ cm^{-1}$, $H=-2JS_1S_2$) determined by variable-temperature magnetic susceptibility measurements was found to be much stronger than in ferromagnetically coupled chromium(III) dimers with a $[Cr^{III}(\mu\text{-}OR)_2(\mu\text{-carboxylato})Cr^{III}]$ core (R = alkyl or H). The magneto-structural correlations developed for the latter compounds cannot be applied to **1** and **2**. However, the sign and magnitude of the exchange coupling appears to be correlated to the size of the bridging Cr–S–Cr angle as also found for the di-μ-alkoxido-bridged species. Our chromium complexes were found to be luminescent. Photoexcitation into the relatively intense thiophenolato-to-Cr^{III} charge transfer and $^4A_2\rightarrow{}^4T_1$ absorption bands ($\lambda_{exc}=405$ nm) produces a broad emission maximum at 750 nm ($\lambda_{max}=750$ nm, $\Phi_L=44$–$45\,\%$, $\tau=121\ \mu s$) attributed to the radiative relaxation from the excited $^2E^4A_2$ state level. These observations may be further exploited for the construction of novel luminescent materials and sensors with magnetic properties.

Experimental Section

Materials and methods

Unless otherwise noted all preparations were carried out under inert conditions. Nitrogen was used as protective gas. The ligand $H_2L\cdot 6HCl$ was prepared as described in the literature. All other reagents were purchased from commercial sources and used without further purification. The IR spectra were measured as KBr disks at $4\ cm^{-1}$ resolution using a Bruker Tensor 27 FTIR spectrometer. UV-vis spectra were recorded on a Jasco V-670 UV-vis/near IR spectrophotometer using 1 cm quartz cells (Hellma). Elemental analysis were determined with a Vario EL – elemental analyzer. ESI-MS spectra were obtained on a Bruker Daltronics Esquire 3000 Plus spectrometer using the positive ion electrospray ionization modus. Diffuse reflectance spectra were collected on a Jasco V-670 UV-vis-NIR spectrophotometer equipped with an ARN-914 absolute reflectance measurement unit, a photomultiplier and a PbS photoconductive cell. Because of strong absorbance, the samples were optically diluted with $BaSO_4$ (~95 wt%), the baseline being recorded with a Spectralon white standard. The diffuse reflectance (R) of the sample was converted to absorbance (T) via the Kubelka-Munk function: $T=(1\text{-}R)^2/(2R)$ implemented in the spectramanager software.[98] Variable temperature magnetic susceptibility measurements on powdered solid samples were carried out using a MPMS 7XL Squid magnetometer (Quantum Design) over a temperature range of 2–200 K at an applied magnetic field of 0.1 and 0.5 Tesla. Variable-temperature-variable-field dc magnetisation experiments were carried out in the 0.5–7.0 T magnetic field ranges at 2 K. The observed susceptibility data were corrected for underlying diamagnetism. Cyclic voltammetry measurements were conducted with an Autolab potentiostat/galvanostat. The cell contained a Pt disk working electrode, a Pt wire auxiliary electrode and a silver wire as reference electrode. Concentrations of solutions were 0.1 M in supporting electrolyte ($[n\text{Bu}_4\text{N}]PF_6$) and ca. 1×10^{-3} M in sample. Ferrocene was used as internal standard.[99]

Caution! Perchlorate salts are potentially explosive and should therefore only be prepared in small quantities and handled with appropriate care.

Synthesis and analysis of compounds

General procedure for complexes 1 and 2

$H_2L\cdot 6HCl$ (192 mg, 0.215 mmol), anhydrous $CrCl_2$ (53 mg, 0.43 mmol, 2 equiv.) and the corresponding coligand L′ (NaOAc·3H2O 29.3 mg, 0.215 mmol, 1 equiv. (for **1**) or LiO_2CPh (28 mg, 0.22 mmol, 1 equiv. (for **2**)) were dissolved in 50 mL methanol. Triethylamine (239 μL, 1.72 mmol, 6 equiv.) was added and the resulting green solution was stirred overnight. The reaction mixture was exposed to air and stirred for an additional hour to complete oxidation of intermediate Cr^{II} complexes. The solution was filtered, a solution of $LiClO_4\cdot 3H_2O$ (606 mg, 4.31 mmol) in EtOH (30 mL) was added, and the solvent volume was reduced under vacuum until precipitation occurred. The resulting solid was collected by filtration, and washed with little ethanol and ether.

$[Cr_2L(\mu\text{-}OAc)](ClO_4)_3$ (**1**): red-brown powder. Yield: 155.0 mg, 64%. MS (ESI+, MeCN): calcd for $C_{40}H_{67}Cl_2Cr_2N_6O_{10}S_2$ $[M\text{–}ClO_4^-]^+$ 1029.25, found 1031.25; calcd. for $C_{40}H_{67}ClCr_2N_6O_6S_2$ $[M - 2ClO_4^-]^{2+}$ 465.16, found 465.17; calcd. for $C_{40}H_{67}Cr_2N_6O_2S_2$ $[M\text{-}3ClO_4^-]^{3+}$ 277.12, found 277.13. Elemental analysis for $C_{40}H_{67}Cl_3Cr_2N_6O_{14}S_2\cdot 2H_2O$ (M = 1130.20 + 36.02) calcd. C, 41.19; H, 6.13; N, 7.20, found C, 41.24; H, 6.01; N, 7.24. IR (KBr): $\tilde{\nu}=3440$ (br, w), 2960 (br, m), 1525 (s), 1501 (m), 1455 (s), 1365 (w), 1305(w), 1244 (w), 1144 (m), 1116 (s), 1098 (s), 1033 (s), 926 (w), 889 (m), 820 (m), 804 (w), 746 (w), 662 (w), 624 (s), 572 (w), 489 (w), 424 (w) cm^{-1}.

$[Cr_2L(\mu\text{-}OPh)](ClO_4)_3$ (**2**): red-brown powder, yield: 176 mg, 69%. MS (ESI+, MeCN): calcd for $C_{45}H_{69}Cl_2Cr_2N_6O_{10}S_2$ $[M\text{–}ClO_4^-]^+$ 1091.27, found 1091.27; calcd. for $C_{45}H_{69}ClCr_2N_6O_6S_2$ $[M - 2ClO_4^-]^{2+}$ 496.17, found 496.16; calcd. for $C_{45}H_{69}Cr_2N_6O_2S_2$ $[M\text{-}3ClO_4^-]^{3+}$ 297.79, found 297.79. Elemental analysis for $C_{45}H_{69}Cl_3Cr_2N_6O_{14}S_2\cdot 2H_2O$ (M = 1192.54 + 36.02) calcd. C, 43.99; H, 5.99; N, 6.84; found C, 43.62; H, 5.78; N, 7.02. IR (KBr): $\tilde{\nu}=3450$ (br, s), 2954 (m), 1628 (w), 1595 (w), 1523 (s), 1468 (m), 1414 (s), 1364 (w), 1310 (w), 1239 (s), 1142 (s), 1117 (s), 1088 (s), 1035 (m), 928 (w), 891 (m), 820 (s), 748 (w), 678 (m), 624 (s), 554 (w), 511 (w) 431 (w) cm^{-1}.

X-ray diffractometry of single crystals

Suitable specimens were selected and mounted on the tip of a glass needle using perfluoropolyether oil. The data sets were collected at 180(2) K on a STOE STADIVARI X-ray diffractometer equipped with an X-ray microsource (Cu-K_α, $\lambda=1.54186$ Å), a multilayer mirror and a Dectris Pilatus-300 K detector. Data processing was carried out with the STOE X-Area software including a spherical absorption correction and scaling routine.[100] The structures were solved with SHELXT 2018/2[101] using dual methods and refined by full matrix least squares minimization on F^2 using version 2018/3 SHELXL[102] and Olex2.[103] The coordinates of all non-hydrogen and non-disordered atoms were refined with anisotropic thermal parameters. Hydrogen atoms were included on idealised positions.

In both crystal structures one *tert*-butyl group and one ClO_4^- ion were found to be disordered over two sites. A split atom model was applied to account for this disorder to give site occupancy factors of 0.67/0.33 (C32,C33,C34 a/b) and 0.69/0.31 (O3,O4,O5,O6

a/b) for **1**·2H_2O and 0.31/0.69 (C32,C33,C34 a/b) and 0.47/0.53 (O7,O8,O9,O10 a/b) for **2**·*x*MeCN (*x* ~4.5), respectively. In the structure of **2**·*x*MeCN (*x* ~4.5) there are ~4.5 MeCN solvate molecules. Three MeCN molecules (per formula unit) could be refined. The other 1.5 MeCN molecules occupy interstitial spaces generated by packing and were found to be highly disordered. This disorder was sufficiently bad to prevent modelling, and so SQUEEZE[104] implemented in Platon was applied to remove diffuse electron density. The total potential solvent accessible void volume per unit cell was determined to be 1828 Å^3 (electron count: 440 electrons corresponding to ~23 MeCN). This corresponds to ~1.5 extra MeCN solvates giving a total of 4.5 MeCN molecules per formula unit. Graphics were produced with Ortep3 for Windows and PovRAY. Table 3 summarizes selected crystallographic data.

Photophysical characterization

Time-resolved photoluminescence spectroscopy was carried out in frozen CH_2Cl_2/MeOH glassy matrices of the complexes **1** and **2** on a FluoTime300 spectrometer from PicoQuant equipped with a 300 W ozone-free Xe lamp (250–900 nm), a 10 W Xe flash-lamp (250–900 nm, pulse width <10 μs) with repetition rates of 0.1–300 Hz, an excitation monochromator (Czerny-Turner 2.7 nm/mm dispersion, 1200 grooves/mm, blazed at 300 nm), diode lasers (pulse width <80 ps) operated by a computer-controlled laser driver PDL-820 (repetition rate up to 80 MHz, burst mode for slow and weak decays), two emission monochromators (Czerny-Turner, selectable gratings blazed at 500 nm with 2.7 nm/mm dispersion and 1200 grooves/mm, or blazed at 1250 nm with 5.4 nm/mm dispersion and 600 grooves/mm), Glan-Thompson polarizers for excitation (Xe-lamps) and emission, a Peltier-thermostatized sample holder from Quantum Northwest (−40 °C–105 °C), and two detectors, namely a PMA Hybrid 40 (transit time spread FWHM <120 ps, 300–720 nm) and a R5509-42 NIR-photomultiplier tube (transit time spread FWHM 1.5 ns, 300–1400 nm) with external cooling (−80 °C) from Hamamatsu. Steady-state spectra and fluorescence lifetimes were recorded in TCSPC mode by a PicoHarp 300 (minimum base resolution 4 ps). Long lifetimes were measured in the MCS mode (NanoHarp). Emission and excitation spectra were corrected for source intensity (lamp and grating) by standard correction curves. Lifetime analysis was performed using the commercial FluoFit software. The quality of the fit was assessed by minimizing the reduced chi squared function ($\chi 2$) and visual inspection of the weighted residuals and their autocorrelation. Luminescence quantum yields were measured with a Hamamatsu Photonics absolute PL quantum yield measurement system (C9920-02) equipped with a L9799-01 CW Xenon light source (150 W), monochromator, C7473 photonic multi-channel analyzer, integrating sphere and employing U6039-05 PLQY measurement software (Hamamatsu Photonics, Ltd., Shizuoka, Japan). All solvents used were of spectrometric grade (Uvasol®).

Table 3. Crystallographic data for **1**·2H_2O and **2**·*x*MeCN (*x* ~4.5).

Compound	**1**·2H_2O	**2**·*x*MeCN (*x* ~4.5)
Formula	$C_{40}H_{75}Cl_3Cr_2N_6O_{16}S_2$	$C_{54}H_{82.5}Cl_3Cr_2N_{10.5}O_{14}S_2$
M_r [g/mol]	1166.5	1377.28
Space group	$P2_1/c$	$P2_1/n$
a, Å	14.727(3)	23.762(5)
b, Å	14.108(3)	16.017(3)
c, Å	25.283(5)	35.243(7)
a deg	90	90
b, deg	98.66(3)	97.16(3)
γ, deg	90	90
V, Å^3	5193(2)	13309(5)
Z	4	8
d_{calcd}, g/cm^3	1.49	1.31
Cryst. size, mm^3	0.10×0.08×0.06	0.38×0.27×0.17
μ(Cu Kα), mm^{-1}	6.244	4.911
2θ limits, deg	1.79–35.4	1.67–35.4
Measured refl.	46228	113147
Independent refl.	9822	25089
Observed refl.[a]	7822	16834
No. parameters/restraints	718/150	1552/297
*R*1[b] (*R*1 all data)	0.0382 (0.0528)	0.0649 (0.0982)
w*R*2[c] (w*R*2 all data)	0.0981 (0.1044)	0.1717 (0.1928)
Max, min peaks, e/Å^3	0.860/−0.606	0.934/−1.50

[a] Observation criterion: $I>2\sigma(I)$. [b] $R1=\Sigma||F_o|-|F_c||/\Sigma|F_o|$. [c] $wR2=\{\Sigma[w(F_o^2-F_c^2)^2]/\Sigma[w(F_o^2)^2]\}^{1/2}$. Deposition Number(s) CCDC-2087606 (for **1**·2H_2O), CCDC-2087607 (for **2**·*x*MeCN), contain(s) the supplementary crystallographic data for this paper. These data are provided free of charge by the joint Cambridge Crystallographic Data Centre and Fachinformationszentrum Karlsruhe Access Structures service.

PLIM (phosphorescence lifetime microscopy) for complex **2** (finely ground powder) was performed with confocal laser scan excitation and time-correlated single photon counting (TPSPC) (DCS-120, Becker & Hickl). A diode laser (405 nm, 60 ps, Becker & Hickl) served as the pulsed laser excitation source. The system was excited until saturation occurred, after which no more excitation was carried out; this process is also known as "burst mode". The light was focused and captured in the backscatter geometry with a 10x objective (Olympus LUCPlan FLN 10x NA = 0.3). A 480 ± 50 nm bandpass filter was used for the selective detection of phosphorescence. In order to determine the phosphorescence lifetime for each data point, the time profile was fitted with a mono-exponential function (SPC Image software, Becker & Hickl).

Steady state photoluminescence spectra for solid samples of **1** and **2** (Figure S18) were obtained with an inverted confocal microscope (IX71, Olympus), fiber-coupled to a spectrometer (iHR320, synapse CCD, HORIBA JobinYvon) with photo excitation at 355 nm (xenon lamp as source). The light was focused and composed in the back-scattering geometry with a 10x objective (Olympus LUCPlan FLN 10x NA = 0.3).

DFT calulations. Density functional theoretical calculations were carried out using the ORCA program package (version 4.2.0).[105] Tight convergence criteria were chosen for all calculations (keyword TightSCF and TightOpt). All calculations make use of the resolution of identity (Split-RI-J) approach for the Coulomb term in combination with the chain-of-spheres approximation for the exchange term (COSX) as implemented in ORCA.[106,107] Grimme's empirical dispersion correction D3(BJ) was employed.[108,109] The geometries of the complex cations were taken from the crystal structures and optimized using the B3LYP functional[110] in combination with Ahlrichs' split-valence triple-ζ-basis set def2-TZVPP and the decontracted def2/J for all atoms.[111,112] All calculations were performed using increased iteration grids (GRID5 NOFINALGRID). Final geometries were checked by numerical frequency calculations for imaginary modes. *J* values were computed from the energy difference between the HS and BS state using the ORCA Brokensym feature. *J* values were calculated according to the Yamaguchi equation (Eq. (5)),

$$J = -\frac{^{HS}E(\chi) - {}^{BS}E(\chi)}{^{HS}\langle S^2\rangle - {}^{BS}\langle S^2\rangle} \quad (5)$$

where ^{HS}E and $^{HS}<S^2>$ correspond to the total energy and total spin angular momentum for the high-spin state (HS), and ^{BS}E and $^{BS}<S^2>$ to the total energy and total spin angular momentum for the broken-symmetry state (BS). This scheme is valid over the whole coupling strengths regime.[113] Convergence to the desired BS solution was confirmed by inspection of orbitals and spin populations.

Supporting Information

Supporting Information available: IR spectra, ESI-MS spectra, magnetic susceptibility data, magnetization plots, plot for structure of **2**, magnetic orbital plots, tabulated Mulliken spin densities and coordinates for computational structures for **1**, **2**, **1′**, **2′**, excitation and emission spectra for **1** and **2**, results of time-resolved decay measurements, CIF-Files for **1** and **2**.

Acknowledgements

We are thankful to Prof. Dr. H. Krautscheid for providing facilities for X-ray crystallographic measurements, and for the Leipzig University Computing Centre for providing facilities for DFT calculations. This work was supported by the Deutsche Forschungsgemeinschaft (DFG priority program SPP2102, "Light Controlled Reactivity of Metal Complexes") and the University of Leipzig. Open Access funding enabled and organized by Projekt DEAL.

Conflict of Interest

The authors declare no conflict of interest.

Keywords: crystal structures · dinuclear chromium(III) complexes · luminescence · magnetic properties · thiolato ligand

[1] a) R. D. Cannon, R. P. White, *Prog. Inorg. Chem.* **1988**, *36*, 195–298; b) U. A. Jayasooriya, R. D. Cannon, R. P. White, J. A. Stride, R. Grinter, G. J. Kearley, *J. Chem. Phys.* **1993**, *98*, 9303–9310.
[2] a) H. Riesen, H. U. Güdel, *Mol. Phys.* **1987**, *60*, 1221–1244; b) P. J. McCarthy, H. U. Güdel, *Coord. Chem. Rev.* **1988**, *88*, 69–131.
[3] T. Ellis, M. Glass, A. Harton, K. Folting, J. C. Huffman, J. B. Vincent, *Inorg. Chem.* **1994**, *33*, 5522–5527.
[4] A. Bino, D. C. Johnston, D. P. Goshorn, T. R. Halbert, E. I. Stiefel, *Science* **1988**, *241*, 1479–1481.
[5] M. Eshel, A. Bino, I. Felner, D. C. Johnston, M. Luban, L. L. Miller, *Inorg. Chem.* **2000**, *39*, 1376–1380.
[6] H. Weihe, H. U. Güdel, H. Toftlund, *Inorg. Chem.* **2000**, *39*, 1351–1362.
[7] A. M. Todea, A. Merca, H. Bögge, J. van Slageren, M. Dressel, L. Engelhardt, M. Luban, T. Glaser, M. Henry, A. Müller, *Angew. Chem. Int. Ed.* **2007**, *46*, 6106–6110; *Angew. Chem.* **2007**, *119*, 6218–6222.
[8] E. J. L. McInnes, C. Anson, A. K. Powell, A. J. Thomson, S. Poussereau, R. Sessoli, *Chem. Commun.* **2001**, 89–90.
[9] D. Foguet-Albiol, T. A. O'Brien, W. Wernsdorfer, B. Moulton, M. J. Zaworotko, K. A. Abboud, G. Christou, *Angew. Chem. Int. Ed.* **2005**, *44*, 897–901; *Angew. Chem.* **2007**, *117*, 919–923.
[10] D. M. Low, G. Rajaraman, M. Helliwell, G. Timco, J. van Slageren, R. Sessoli, S. T. Ochsenbein, R. Bircher, C. Dobe, O. Waldmann, H. U. Güdel, M. A. Adams, E. Ruiz, S. Alvarez, E. J. L. McInnes, *Chem. Eur. J.* **2006**, *12*, 1385–1396.
[11] E. J. McInnes, G. A. Timco, G. F. Whitehead, R. E. Winpenny, *Angew. Chem. Int. Ed.* **2015**, *54*, 14244–14269; *Angew. Chem.* **2015**, *127*, 14450–14477.
[12] M. Jurić, L. Androš Dubraja, D. Pajić, F. Torić, A. Zorko, A. Ozarowski, V. Despoja, W. Lafargue-Dit-Hauret, X. Rocquefelte, *Inorg. Chem.* 2017, 56, 6879–6889.
[13] S. K. Langley, C. M. Forsyth, B. Moubaraki, K. S. Murray, *Dalton Trans.* **2015**, *44*, 912–915.
[14] A. Døssing, *Coord. Chem. Rev.* **2014**, *280*, 38–53.
[15] F. Tuczek, E. I. Solomon, *Coord. Chem. Rev.* **2001**, *219–221*, 1075–1112.
[16] a) L. S. Forster, *Chem. Rev.* **1990**, *90*, 331–353; b) L. S. Forster, *Coord. Chem. Rev.* **2002**, *227*, 59–92.
[17] A. D. Kirk, *Chem. Rev.* **1999**, *99*, 1607–1640.
[18] N. A. P. Kane-Maguire, *Top. Curr. Chem.* **2007**, *280*, 37–67.
[19] S. Treiling, C. Wang, C. Förster, F. Reichenauer, J. Kalmbach, P. Boden, J. P. Harris, L. Carrella, E. Rentschler, U. Resch-Genger, C. Reber, M. Seitz, M. Gerhards, K. Heinze, *Angew. Chem. Int. Ed.* **2019**, *58*, 18075–18085; *Angew. Chem.* **2019**, *131*, 18243–18253.
[20] R. Schenker, H. Weihe, H. U. Güdel, *Inorg. Chem.* **1999**, *38*, 5593–5601.
[21] L. Mønsted, O. Mønsted, J. Springborg, *Inorg. Chem.* **1985**, *24*, 3496–3498.
[22] T. F. Tekut, C. J. O'Connor, R. A. Holwerda, *Inorg. Chem.* **1993**, *32*, 324–328.
[23] T. J. Morsing, J. Bendix, H. Weihe, A. Dossing, *Inorg. Chem.* **2014**, *53*, 2996–3003.
[24] H. Riesen, C. Reber, H. U. Güdel, K. Wieghardt, *Inorg. Chem.* **1987**, *26*, 2747–2750.
[25] J. Glerup, S. Larsen, H. Weihe, *Acta Chem. Scand.* **1993**, *47*, 1154–1161.
[26] H. W. L. Fraser, G. S. Nichol, G. Velmurugan, G. Rajaraman, E. K. Brechin, *Dalton Trans.* **2017**, *46*, 7159–7168.
[27] B. Briat, M. F. Russel, J. C. Rivoal, J. P. Chapelle, O. Kahn, *Mol. Phys.* **1977**, *34*, 1357–1389.
[28] P. Kögerler, B. Tsukerblat, A. Müller, *Dalton Trans.* **2010**, *39*, 21–36.
[29] A. Dei, D. Gatteschi, L. Pardi, U. Russo, *Inorg. Chem.* **1991**, *30*, 2589–2594.
[30] D. Guo, J. K. McCusker, *Inorg. Chem.* **2007**, *46*, 3257–3274.
[31] C. Hua, J. A. DeGayner, T. D. Harris, *Inorg. Chem.* **2019**, *58*, 7044–7053.
[32] J. Glerup, D. J. Hodgson, E. Pedersen, *Acta Chem. Scand. Ser. A* **1983**, *37*, 161–164.
[33] A. Cornia, A.-L. Barra, V. Bulicanu, R. Clérac, M. Cortijo, E. A. Hillard, R. Galavotti, A. Lunghi, A. Nicolini, M. Rouzières, L. Sorace, F. Totti, *Inorg. Chem.* **2020**, *59*, 1763–1777.
[34] E. D. Estes, R. P. Scaringe, W. E. Hatfield, D. J. Hodgson, *Inorg. Chem.* **1976**, *15*, 1179–1182.
[35] C. Reber, H. U. Güdel, L. Spiccia, W. Marty, *Inorg. Chem.* **1987**, *26*, 3186–3191.
[36] R. Sanzenbacher, A. Bottcher, H. Elias, M. Huber, W. Haase, J. Glerup, T. B. Jensen, M. Neuburger, M. Zehnder, J. Springborg, C. E. Olsen, *Inorg. Chem.* **1996**, *35*, 7493–7499.
[37] H. W. L. Fraser, L. Smythe, S. Dey, G. S. Nichol, S. Piligkos, G. Rajaraman, E. K. Brechin, *Dalton Trans.* **2018**, *47*, 8100–8109.
[38] V. Lozan, C. Loose, J. Kortus, B. Kersting, *Coord. Chem. Rev.* **2009**, *253*, 2244–2260.
[39] B. Kersting, G. Steinfeld, *Chem. Commun.* **2001**, 1376–1377.
[40] V. Lozan, B. Kersting, *Inorg. Chem.* **2008**, *47*, 5386–5393.
[41] U. Lehmann, J. Klingele, V. Lozan, G. Steinfeld, M. H. Klingele, S. Käss, A. Rodenstein, B. Kersting, *Inorg. Chem.* **2010**, *49*, 11018–11029.
[42] M. Golecki, B. Kersting, *Z. Anorg. Allg. Chem.* **2015**, *641*, 436–441.
[43] R. Schnitter, D. Gallego, B. Kersting, *Dalton Trans.* **2014**, *43*, 13637–13648.
[44] J. Lach, A. Jeremies, D. Breite, B. Abel, B. Mahns, M. Knupfer, V. Matulis, O. A. Ivashkevich, B. Kersting, *Inorg. Chem.* **2014**, *53*, 10825–10834.
[45] M. Golecki, B. Kersting, *Z. Anorg. Allg. Chem.* **2013**, *639*, 2473–2481.
[46] M. Golecki, J. Lach, A. Jeremies, F. Lungwitz, M. Fronk, G. Salvan, D. R. T. Zahn, J. Park, Y. Krupskaya, V. Kataev, R. Klingeler, B. Büchner, B. Mahns, M. Knupfer, P. F. Siles, O. G. Schmidt, A. Reis, W. R. Thiel, D. Breite, B. Abel, B. Kersting, *Chem. Eur. J.* **2013**, *19*, 7787–7801.
[47] T. Glaser, Y. Journaux, G. Steinfeld, V. Lozan, B. Kersting, *Dalton Trans.* **2006**, 1738–1748.
[48] B. Kersting, G. Steinfeld, *Inorg. Chem.* **2002**, *41*, 1140–1150.
[49] G. Steinfeld, V. Lozan, B. Kersting, *Angew. Chem. Int. Ed.* **2003**, *42*, 2261–2263; *Angew. Chem.* **2003**, *115*, 2363–2365.
[50] U. Lehmann, J. Lach, F. Schleife, A. Jeremies, B. Kersting *Eur. J. Inorg. Chem.* **2013**, *2013*, 1336–1350.
[51] G. Siedle, B. Kersting, *Z. Anorg. Allg. Chem.* **2006**, *632*, 763–770.
[52] R. Schenker, H. Weihe, H. U. Güdel, B. Kersting, *Inorg. Chem.* **2001**, *40*, 3355–3362.
[53] S. Otto, M. Grabolle, C. Förster, C. Kreitner, U. Resch-Genger, K. Heinze, *Angew. Chem. Int. Ed.* **2015**, *54*, 11572–1156; *Angew. Chem.* **2015**, *127*, 11735–11739.
[54] K. Nakamoto, *Infrared and Raman Spectra of Inorganic and Coordination Compounds*, 5th ed., Wiley, New York, **1997**.
[55] G. B. Deacon, R. J. Philipp, *Coord. Chem. Rev.* **1980**, *33*, 227–250.
[56] T. Beissel, T. Glaser, F. Kesting, K. Wieghardt, B. Nuber, *Inorg. Chem.* **1996**, *35*, 3936–3947.

[57] P. V. Bernhardt, P. Comba, N. F. Curtis, T. W. Hambley, G. A. Lawrance, M. Maeder, A. Siriwardena, *Inorg. Chem.* **1990**, *29*, 3208–3213.
[58] C. A. Grapperhaus, M. Y. Darensbourg, *Acc. Chem. Res.* **1998**, *31*, 451–459.
[59] M. Gennari, M. Orio, J. Pécaut, E. Bothe, F. Neese, M.-N. Collomb, C. Duboc, *Inorg. Chem.* **2011**, *50*, 3707–3761.
[60] B. Cordero, V. Gómez, A. E. Platero-Prats, M. Revés, J. Echeverría, E. Cremades, F. Barragán, S. Alvarez, *Dalton Trans.* **2008**, 2832–2838.
[61] S. Merlino, F. Sartori, *Acta Crystallogr., Sect. B: Struct. Crystallogr. Cryst. Chem.* **1972**, *28*, 972–976.
[62] C. L. Raston, A. H. White, *Aust. J. Chem.* **1977**, *30*, 2091–2094.
[63] J. I. Bruce, L. R. Gahan, T. W. Hambley, R. Stranger, *J. Chem. Soc. Chem. Commun.* **1993**, 702–704.
[64] K. Shiren, K. Tanaka, *Inorg. Chem.* **2002**, *41*, 5912–5919.
[65] J. R. Nicholson, G. Christou, R. J. Wang, J. C. Huffman, H.-R. Chang, D. N. Hendrickson, *Polyhedron* **1991**, *10*, 2255–2263.
[66] C. P. Rao, J. R. Dorfman, R. H. Holm, *Inorg. Chem.* **1986**, *25*, 428–439.
[67] N. F. Chilton, R. P. Anderson, L. D. Turner, A. Soncini, K. S. Murray, *J. Comput. Chem.* **2013**, *34*, 1164–1175.
[68] We also tried to fit the susceptibility data by inclusion of an axial zero-field parameter (*D*) parameter in the Hamiltonian 3. This also improved the fits, but the obtained *D* values ($|D| = 0.60$ cm^{-1} (**1**), 0.50 cm^{-1} (**2**)) are much larger than those typically observed for octahedral Cr(III) complexes. It is know that temperature dependent magnetic susceptibility measurements are not very appropriate for the determination of *D* values, see a) A. Meyer, A. Gleizes, J.-J. Girerd, M. Verdaguer, O. Kahn, *Inorg. Chem.* **1982**, *21*, 1729–1739; b) R. Herchel, R. Boca, J. Krzystek, A. Ozarowski, M. Duran, J. van Slageren, *J. Am. Chem. Soc.* **2007**, *129*, 10306–10307.
[69] B. Feldscher, A. Stammler, H. Bögge, T. Glaser, *Chem. Asian J.* **2014**, *9*, 2205–2218.
[70] B. Feldscher, H. Theil, A. Stammler, H. Bögge, T. Glaser, *Inorg. Chem.* **2021**, *51*, 8652–8654.
[71] T. J. Morsing, H. Weihe, J. Bendix, *Eur. J. Inorg. Chem.* **2014**, *2014*, 5990–5996.
[72] D. A. Pantazis, *J. Chem. Theory Comput.* **2019**, *15*, 938–948.
[73] D. E. Bolster, P. Gütlich, W. E. Hatfield, S. Kremer, E. W. Müller, K. Wieghardt, *Inorg. Chem.* **1983**, *22*, 1725–1729.
[74] K. Wieghardt, P. Chaudhuri, B. Nuber, J. Weiss, *Inorg. Chem.* **1982**, *21*, 3086–3090.
[75] O. Kahn, *Molecular Magnetism*, Wiley VCH, New York, **1993**.
[76] A. Jeremies, S. Gruschinski, M. Meyer, V. Matulis, O. A. Ivashkevich, K. Kobalz, B. Kersting, *Inorg. Chem.* **2016**, *55*, 1843–1853.
[77] A. Jeremies, U. Lehmann, S. Gruschinski, V. Matulis, O. A. Ivashkevich, A. Jäschke, B. Kersting, *J. Organomet. Chem.* **2016**, *821*, 171–181.
[78] J. Klose, A. Jeremies, T. Severin, D. Fuhrmann, J. Bergmann, J. Griebel, B. Abel, B. Kersting, *Beilstein J. Org. Chem.* **2019**, *15*, 840–851.
[79] S. Otto, C. Förster, C. Wang, U. Resch-Genger, K. Heinze, *Chem. Eur. J.* **2018**, *24*, 12555–12563.
[80] L. A. Büldt, X. Guo, R. Vogel, A. Prescimone, O. S. Wenger, *J. Am. Chem. Soc.* **2017**, *139*, 985–992.
[81] E. Previtera, A. Tissot, *Eur. J. Inorg. Chem.* **2016**, *2016*, 1972–1979.
[82] A. Cadranel, P. S. Oviedo, P. Alborés, L. M. Baraldo, D. M. Guldi, J. H. Hodak, *Inorg. Chem.* **2018**, *57*, 3042–3053.
[83] P. T. Burks, A. D. Ostrowski, A. A. Mikhailovsky, E. M. Chan, P. S. Wagenknecht, P. C. Ford, *J. Am. Chem. Soc.* **2012**, *134*, 13266–13275.
[84] L. Aboshyan-Sorgho, C. Besnard, P. Pattison, K. R. Kittilstved, A. Aebischer, J.-C. G. Bünzli, A. Hauser, C. Piguet, *Angew. Chem. Int. Ed.* **2011**, *50*, 4108–4112; *Angew. Chem.* **2011**, *123*, 4194–4198.
[85] The term symbols $^4T_2$, ^2E, etc., of the *O* point group are employed here but it should be kept in mind that the actual symmetry of the complexes is much lower (if there is symmetry at all). This level of approximation implies that the $^2E^4A_2$ and $^2T_1{}^4A_2$ states are degenerate, which is clearly not the case (Figure 3).
[86] H. U. Güdel, L. Dubicki, *Chem. Phys. Lett.* **1974**, *6*, 272–281.
[87] A. L. Hale, W. Levason, *J. Chem. Soc. Dalton Trans.* **1983**, 2569–2571.
[88] A. B. P. Lever, *J. Chem. Educ.* **1968**, *45*, 711–712.
[89] P. S. Wagenknecht, C. Hu, D. Ferguson, L. C. Nathan, R. D. Hancock, J. R. Whitehead, K. Wright-Garcia, M. T. Vagnini, *Inorg. Chem.* **2005**, *44*, 9518–9526.
[90] P. S. Wagenknecht, P. C. Ford, *Coord. Chem. Rev.* **2011**, *255*, 591–616.
[91] J. Ferguson, H. J. Guggenheim, Y. Tanabe, *J. Phys. Soc. Jpn.* **1966**, *21*, 692–704.
[92] In the case of exchange-coupled dinuclear chromium(III) complexes, the ground state ($^4A_2{}^4A_2$) will have four levels with total spin $S = 3, 2, 1, 0$, while the lowest singly excited states arising from the ($^2E^4A_2$) configuration will have two levels with total spin $S^* = 1, 2$, giving rise to several spin-allowed absorption bands.
[93] W. J. Mitchell, M. K. DeArmond, *J. Lumin.* **1971**, *4*, 137–148.
[94] A. Ditze, F. Wasgestian, *Ber. Bunsen-Ges.* **1986**, *90*, 111.
[95] K. N. Brown, R. J. Geue, G. Moran, S. F. Ralph, H. Riesen, A. M. Sargeson, *Chem. Commun.* **1998**, 2291–2292.
[96] N. A. P. Kane-Maguire, K. C. Wallace, D. B. Miller, *Inorg. Chem.* **1985**, *24*, 597–605.
[97] A. D. Kirk, G. B. Porter, *J. Phys. Chem.* **1980**, *84*, 887–891.
[98] G. Kortüm, *Reflexionsspektroskopie: Grundlagen, Methodik, Anwendungen*, Springer, Berlin, **1969**.
[99] N. G. Connelly, W. E. Geiger, *Chem. Rev.* **1996**, *96*, 877–910.
[100] Stoe & Cie GmbH, *X-AREA, X-RED32, X-SHAPE and LANA*, Stoe & Cie, Darmstadt, Germany, **2019**.
[101] G. M. Sheldrick, *Acta Crystallogr., Sect A: Found. Adv.* **2015**, *71*, 3–8.
[102] G. M. Sheldrick, *Acta Crystallogr., Sect C: Struct. Chem.* **2015**, *71*, 3–8.
[103] O. V. Dolomanov, L. J. Bourhis, R. J. Gildea, J. A. K. Howard, H. Puschmann, *J. Appl. Crystallogr.* **2009**, *42*, 339–341.
[104] A. L. Spek, *PLATON - A Multipurpose Crystallographic Tool*, Utrecht University, Utrecht, The Netherlands, **2000**.
[105] F. Neese, *Wiley Interdiscip. Rev.: Comput. Mol. Sci.* **2012**, *2*, 73–78.
[106] F. Neese, F. Wennmohs, A. Hansen, U. Becker, *Chem. Phys.* **2009**, *356*, 98–109.
[107] R. Izsák, F. Neese, *J. Chem. Phys.* **2011**, *135*, 144105.
[108] S. Grimme, J. Antony, S. Ehrlich, H. Krieg, *J. Chem. Phys.* **2010**, *132*, 154104.
[109] S. Grimme, S. Ehrlich, L. Goerigk, *J. Comput. Chem.* **2011**, *32*, 1456–1465.
[110] A. D. Becke, *J. Chem. Phys.* **1993**, *98*, 5648–5652.
[111] F. Weigend, R. Ahlrichs, *Phys. Chem. Chem. Phys.* **2005**, *7*, 3297–3305.
[112] F. Weigend, *Phys. Chem. Chem. Phys.* **2006**, *8*, 1057–1065.
[113] T. Soda, Y. Kitagawa, T. Onishi, Y. Takano, Y. Shigeta, H. Nagao, Y. Yoshioka, K. Yamaguchi, *Chem. Phys. Lett.* **2000**, *319*, 223–230.

Manuscript received: June 11, 2021
Accepted manuscript online: September 7, 2021
Version of record online: October 6, 2021

